An Investigation on the Performance of Current Derivative Sensors for the Sensorless Control of A.C. Drives

James Borg Bartolo*, Cyril Spiteri Staines*, Cedric Caruana*

* Department of Industrial Electric Power Conversion,
University of Malta,
Tal-Qroqq Malta

Keywords: Sensorless Control, Current Derivative, Saturation .

Abstract: This paper considers different types of current derivative sensors that may be used for tracking the saturation saliency in a.c. machines. The saliency is tracked by measuring the current derivative resulting from voltage 'test' vector application. The performance of different sensors proposed in the literature is investigated.

1 Introduction

This paper investigates different forms of inexpensive current sensors to facilitate the implementation of sensorless control algorithms in AC drives. It has been shown in the literature [1],[2] that the current derivative resulting from the application of a voltage test vector, contains rotor/flux position information. Different approaches for measuring the current derivative were suggested in the literature ranging from its computation from successive current samples[5] to the use of specific sensors like the non integrating Rogowski coil[1] and the coaxial transformer[3].
This paper aims at investigating the performance of a number of current derivative sensors. This study uses voltage test vectors and measures the resulting line current derivatives (using specially designed coils), to extract the position information. The sensors are tested on an off–the–shelf induction machine.

2 Position Estimation Method

The proposed method for position estimation uses voltage test vectors, imposed during the fundamental zero voltage vectors at a rate of 416 Hz. A short duration (28μs or less) voltage vector is applied followed immediately by its inverse [1]e.g. taking vector pair $\mathbf{u}_1$-$\mathbf{u}_4$ from state vector diagram shown below in fig.1.

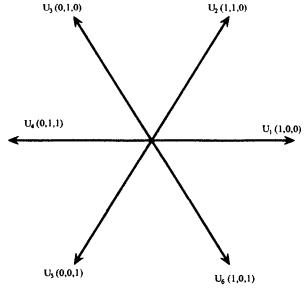

Fig1. Voltage Test Vectors

This is done so as not to effect the fundamental voltage time area. Failure to do so will bring about a resultant fundamental flux density distortion, which will effect the fundamental operation of the machine. Due to the high frequency nature of the injected pulses, the leakage flux paths on the stator are excited. The observed effect is a modulation of the stator leakage reactance and is generally given by [2]:

$$l_{\sigma a} = l_{\sigma 0} + l_{\Delta} \cos(n\theta) \quad (1a)$$

$$l_{\sigma b} = l_{\sigma 0} + l_{\Delta} \cos\left(n\left(\theta - \frac{2\pi}{3}\right)\right) \quad (1b)$$

$$l_{\sigma c} = l_{\sigma 0} + l_{\Delta} \cos\left(n\left(\theta - \frac{4\pi}{3}\right)\right) \quad (1c)$$

where: $l_{\sigma 0}$ is the average inductance and l_{Δ} is the variation in magnitude due to the rotor anisotropy or saturation flux. 'n' assumes a value of 2 for saturation induced anisotropy or $n=N_r/p$ for rotor slotting were N_r is the rotor slot number and p the pole pairs. θ is flux reference angle and assumes of θ_e for the saturated case and θ_r when considering the anisotropy arising from rotor slotting saliency.
Consider the machine to be connected in star (the same method of analysis can be applied to a machine connected in a delta configuration), and that the applied vector is $\mathbf{u}_1(1,0,0)$. During this condition, S1, S4 and S6 are conducting and the positive DC rail is effectively connected to phase ***a***, whilst both ***b*** and ***c*** are shorted to the negative DC rail as shown in Fig.2.

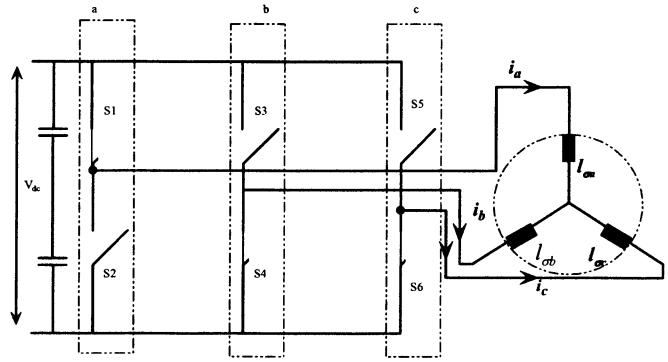

Fig.2. Schematic representation of the motor load showing the leakage inductances connected in star along with the inverter in switching state $\mathbf{u}_1$.

Assuming a relatively slow change in position and using $v_{dc} = l(n\theta) \bullet di/dt$, the derivative of the current impressed in each winding can be expressed in terms of both voltage vector applied and the position dependant leakage inductance by using equations (1).

For the above case (vector $\mathbf{u}_1$):

$$\frac{di_{a(u_1)}}{dt} = \frac{1}{K}\left(2 - \frac{l_\Delta}{l_{\sigma 0}}\cos(n\theta)\right) \quad (2a)$$

$$\frac{di_{b(u_1)}}{dt} = -\frac{1}{K}\left(1 + \frac{l_\Delta}{l_{\sigma 0}}\cos\left(n\left(\theta - \frac{4\pi}{3}\right)\right)\right) \quad (2b)$$

$$\frac{di_{c(u_1)}}{dt} = -\frac{1}{K}\left(1 + \frac{l_\Delta}{l_{\sigma 0}}\cos\left(n\left(\theta - \frac{2\pi}{3}\right)\right)\right) \quad (2c)$$

where :

$$\frac{1}{K} = \frac{v_{dc}}{3l_{\sigma 0}\left(1 - \left(\frac{l_\Delta}{2_{\sigma 0}}\right)\right)} \quad (2d)$$

It follows that a position signal can be extracted from measurement of the current derivatives.

Thus considering the equations derived in (2) for the active switching vector ($\mathbf{u}_1$), the phase position components of the position vector can be expressed as:

$$p_{a(u_1)} = \frac{l_\Delta}{l_{\sigma 0}}\cos(n\theta) = -K.\frac{di_{a(u_1)}}{dt} + 2 \quad (3a)$$

$$p_{b(u_1)} = \frac{l_\Delta}{l_{\sigma 0}}\cos\left(n\left(\theta - \frac{2\pi}{3}\right)\right) = -K.\frac{di_{c(u_1)}}{dt} - 1 \quad (3b)$$

$$p_{c(u_1)} = \frac{l_\Delta}{l_{\sigma 0}}\cos\left(n\left(\theta - \frac{4\pi}{3}\right)\right) = -K.\frac{di_{b(u_1)}}{dt} - 1 \quad (3c)$$

This derivation may be repeated for all active switching states ($\mathbf{u}_1$-$\mathbf{u}_6$) resulting in 18 position components (one per phase per vector/switching state). The position signals exhibit a dc offset as shown in (3). This effect is compensated for by using various combinations of the above derived position components to construct phase position components p_a, p_b and p_c as shown in (4).In the present set up, a pair of voltage test vectors (these being $\mathbf{u}_1$-$\mathbf{u}_4$;$\mathbf{u}_5$-$\mathbf{u}_2$;$\mathbf{u}_3$-$\mathbf{u}_6$) are injected at the beginning of every fundamental PWM cycle as shown in Fig.3.Nine relevant position signals are extracted during vectors $\mathbf{u}_1$;$\mathbf{u}_3$;$\mathbf{u}_5$ resulting in phase position components p_a, p_b, p_c given by:

$$p_a = 1/3.(p_{a(u_1)} + p_{a(u_3)} + p_{a(u_5)}) \quad (4a)$$

$$p_b = 1/3.(p_{b(u_1)} + p_{b(u_3)} + p_{b(u_5)}) \quad (4b)$$

$$p_c = 1/3.(p_{c(u_1)} + p_{c(u_3)} + p_{c(u_5)}) \quad (4c)$$

As the phase position components p_a, p_b and p_c are spatially displaced by $2\pi/3$ radians the resultant position vector p_{res} for flux position estimation is given by:

$$P_{res} = C.(p_a + ap_b + a^2p_c) = p_a + jp_\beta \quad (5)$$

where: p_{res} is the resultant vector, p_a p_b p_c are the above mentioned phase position components, 'a' is a complex operator of unit magnitude and phase of $2\pi/3$ radians. p_α and p_β are the quadrature components in the stationary frame α-β. p_{res} is then calculated by substituting the values obtained from (4) into (5) thus obtaining the resultant quadrature components of the stationary frame p_α p_β in terms of the current derivatives given in (3).The Estimated Flux angle (λ), for the case of saturation saliency, is then obtained from :

$$\lambda = \frac{1}{2}\tan^{-1}(p_\alpha / p_\beta) \quad (6)$$

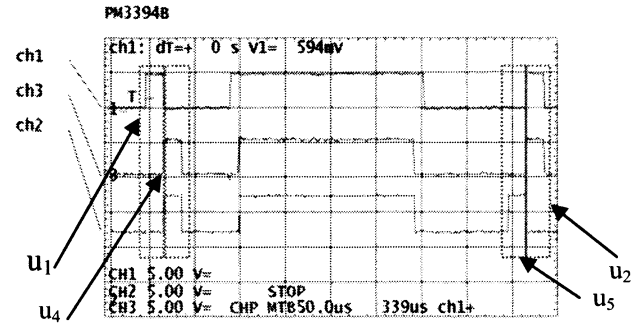

Fig.3. PWM output showing injection sequence $\mathbf{u}_1$-$\mathbf{u}_4$ and $\mathbf{u}_5$-$\mathbf{u}_2$.

3 Experimental Setup

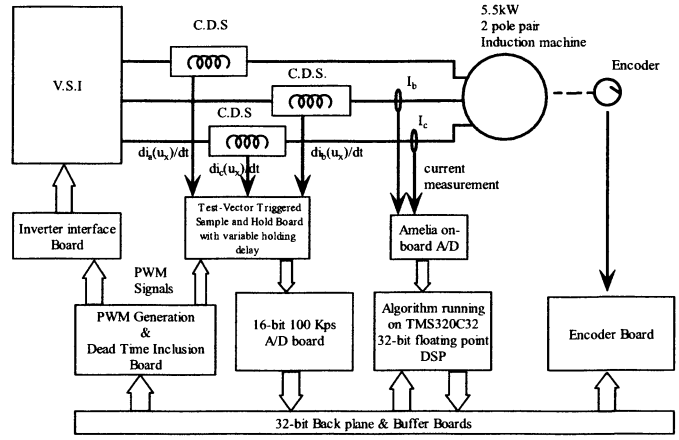

Fig 4. Experimental setup

Fig.4 shows the basic layout of the experimental rig. A standard star connected 5.5kW 4-pole induction motor; is controlled via the slip control algorithm running on a TMS320C32 DSP. A voltage signal proportional to the derivative of current passing to the motor is produced by the Current Derivative Sensors (CDS). A sample and hold circuit was built to synchronise the capture instant with the voltage vector injection. This circuit also provided for a settable time delay t_d between rising edge of the voltage and trigger for the sample and hold IC. This delay was introduced to allow for the current derivative signal to settle. The PWM switching frequency is set to 5 kHz and has a settable dead time of 2.5μs.

4 The Current derivative sensors

Two current derivative sensor topologies were investigated based on those described in [3] and [6] respectively.

The first prototype built was based on [3] and is made out of five turns of coaxial cable mounted on a plastic pipe, see figure 5. The phase current is conducted on the outer sheet and acts as a primary winding; the signal is then measured across the inner core which acts as the sensor's secondary winding. One sensor is applied per phase. Being air- cored there is no risk of saturation, and the induced voltage at the coil end, for any given phase '**m**', during the application of any vector $\mathbf{u}_k$, (k=1→6) ,can be given by the ideal transformer equation as:

$$V_{di_m(u_k)} = \frac{-N_2 N_1 A_{csa}\mu(B,H)}{l_c(N)} \bullet \frac{di_{m(u_k)}}{dt} \quad (7)$$

where: μ(B,H) is the effective magnetic permeability of the core material. It can assume a value of $\mu_o = 4\pi \times 10^{-7}$ H/m if the core is made out of paramagnetic materials such as air, in the case of the coax sensor. The primary and secondary turns are represented in (7) by N_1 and N_2. A_{csa} is the surface area of the flux linkage path, in the case of the coax sensor this becomes the cross-sectional area of the plastic pipe. l_c(N) is the coil length and $di_{m(uk)}/dt$ is the derivative of the '**m**' phase current when the voltage test vector $\boldsymbol{u_k}$ is applied ($\boldsymbol{k}$=1→6).

Detailed modelling of the complete coaxial-based CDS system shows that the measured voltage is also a function of the parasitic effects which exist due to its winding and measurement cable. The latter introduce further zeros and poles into the system which drastically alter the system response. Thus precise tuning of the system is required in order to yield the fastest response with least amount of oscillations on application of a voltage test vector [4]. The CDS output dynamics is further effected by the machine's parasitics. The CDS's output voltage is required to follow to the primary current derivative as accurately as possible. Other types of coaxial-based CDS were constructed, one having 3 turns and the other having an effective turns ratio of 5:20.

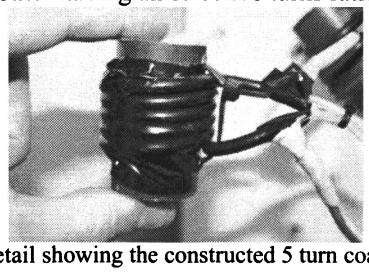

Fig 5. Detail showing the constructed 5 turn coax sensor

The second topology investigated was based on the one described in [6] see figure 6. In the prototypes constructed a toroidal ferrite core was used, linking the secondary winding with the radial flux created by the primary phase winding. The first prototype constructed had a powdered iron core ferrite, turns ratio of 1:20, and no air gap was introduced, retaining the original B-H curve characteristics. The sensor did not exhibit a satisfactory performance due to saturation.

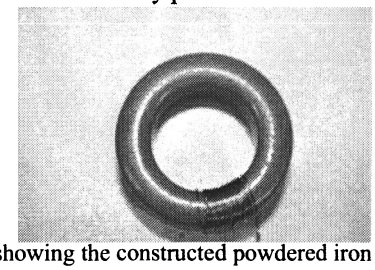

Fig.6. Detail showing the constructed powdered iron toroidal ferrite core. The sensor is mounted directly on the phase conductor thus forming a single turn at the primary.

5 Testing of Current Derivative Sensors

Experiments were first carried out to determine the performance of the CDS. A variable current source was used to investigate their response upon application of a linear current waveform having a *di/dt* of 0.07A/us. The required gradient was calculated from the actual motor current observed upon application of the test vectors. Fig. 7 shows the current test signal applied to the sensors. The falling edge of the current waveform was used to compare the dynamics of the sensors. The main criterion used for performance assessment at this stage was the settling time required for a stable voltage output.

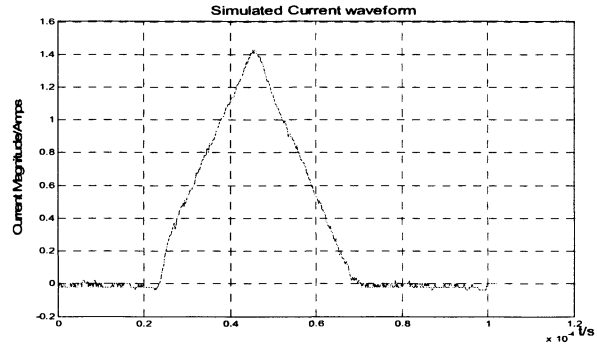

Fig.7.Sythesised current waveform, note slope of 1.4 amps per 20μs, or 70000A/s.

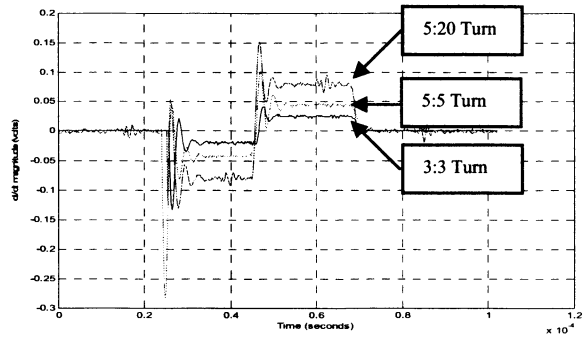

Fig.8. Plot showing the family of responses obtained by the three different coaxial coils implemented

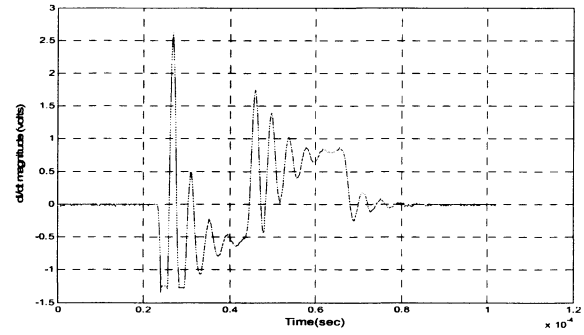

Fig.9. Plot showing the oscillatory response of the CDS wound on a powdered iron toroid.

Figure 8 shows the performance of three different configurations of coaxial CDS .The output voltage for the 3:3 and 5:5 turn coils , is given at 28mV and 45 mV with settling times of 9.5μs and 10.3μs respectively. The third coaxial sensor investigated had at turns ratio of 5:20. With 20 turns at its secondary, the latter had a settling time of 10.4μs and an output voltage of 80mV. Fig. 9. shows the response of a CDS made from a toroidal ferrite core. Although the flux derivative in this coil produced a voltage of relatively higher magnitude, the core response was very oscillatory making this

particular ferrite core unsuitable for use in current derivative measurements.

Further research and experimental tests were carried out on other types of ferrite cores especially those used for high frequency applications. It was found that a much better response could be obtained by changing the material of the toroidal core from powdered iron, to a Mn-Zn alloy. A second prototype having 10 turns wound on a toroidal Mn-Zn core, was then constructed. Other, off-the-shelf, high bandwidth current transducers were also tested and implemented on the test rig in order to evaluate the possibility of using cheap readily available components instead of in house developed transducers. These commercial sensors had a turns ratio of 1:100 and were wound on a toroidal ferrite core.

Following the above performance tests, the sensors selected for implementation on the drive were the coaxial type, the Mn-Zn toroidal type and the commercial high bandwidth type.

6 Experimental Testing of CDS for Flux Position tracking

The experimental set-up of fig 4 was used; where: t_d was set to 26μs, the voltage test vector had duration of 28μs and the injection frequency was set at 416.66Hz.

The output of the sensors was tested to provide a usable $2f_e$ signal suitable for drive orientation.

Figures 10 to 15 show the results obtained with the 5:5 turn coax and the 1:10 turn Mn-Zn ferrite core. The position signals were filtered by means of a 1st order low-pass 10Hz Butterworth filter. The machine's fundamental frequency was set at 3.3Hz (100 rpm) yielding a $2f_e$ signal of 6.67Hz at 30% rated load. The same experimental setup was used to test the 1:100Turn 'off-the-shelf' current transducer.

Figures 10, 13 and 16 show the quadrature position components $\mathbf{p}_\alpha$ and $\mathbf{p}_\beta$ in the time domain for the Coax, Mn-Zn and off-the-shelf sensors respectively. The Mn-zn quadrature components show much larger amplitude when compared to the Coax results. On the other hand preliminary results for the 1:100Turn commercial sensors show a further increase in the quadrature component magnitude when compared to the Mn-Zn case this might be due to an increase in turns ratio.

Figures 11, 14 and 17, show the spectra of one of the quadrature components, for the position vector obtained for the three types of sensors. It is important to note the relatively large magnitude of the $2f_e$ spectral component (at 6.67Hz) present in all of the plots. The alpha component is shown for the Coax and Mn-Zn case. As anticipated from the time domain plots the spectra show that the 2fe component increases substantially for the Mn-Zn sensor. Fig17. shows the spectrum of the beta component obtained for the 1:100Turn transducer. This result shows that even this sensor demonstrates potential for saturation saliency tracking, after further hardware tuning is carried out.

Figures12 and 16 show the successful reconstruction of the resultant flux angle (λ) from quadrature position components $\mathbf{p}_\alpha$ and $\mathbf{p}_\beta$ for the Coax and Mn-Zn sensors respectively.

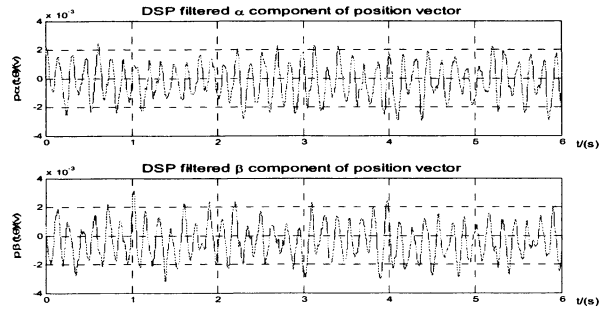

Fig.10. Quadrature components of the resulting position signal shown in the time domain obtained for the 5:5 turn coax sensor.

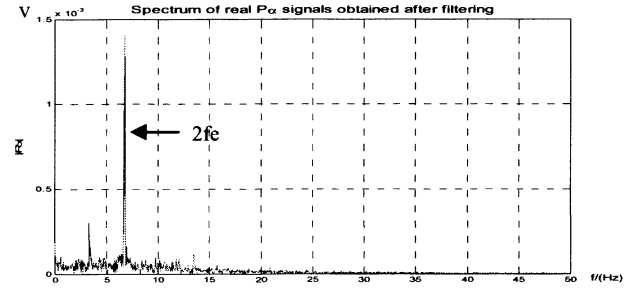

Fig.11. Spectrum of $\mathbf{p}_\alpha$ component obtained for the 5:5 turn coax sensor. The spectrum of the beta component $\mathbf{p}_\beta$ is identical to that of the alpha component shown above.

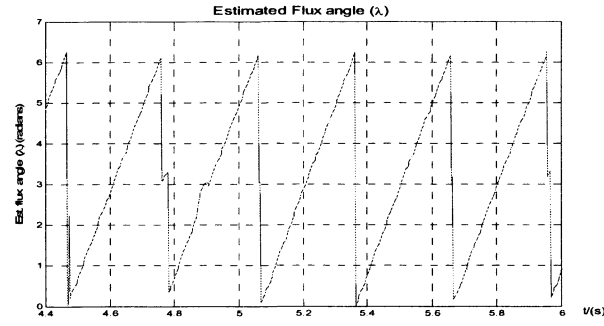

Fig.12. Resulting Flux position angle reconstructed from the 2λ angle obtained naturally from $\mathbf{p}_\alpha$ and $\mathbf{p}_\beta$ for the Coax sensor.

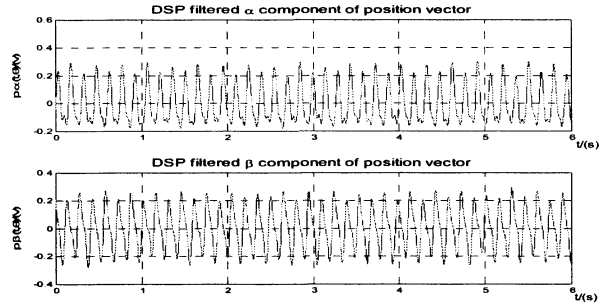

Fig.13. Quadrature components of the resulting position signal shown in the time domain obtained for the 1:10Turn MnZn ferrite sensor.

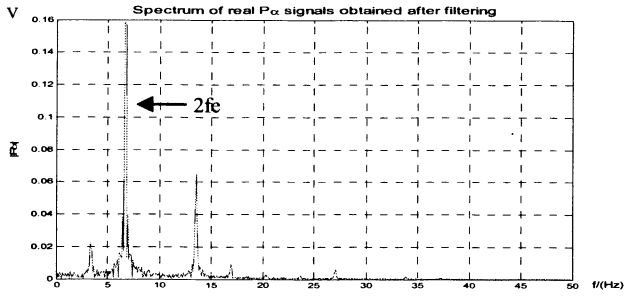

Fig.14. Spectrum of $\mathbf{p}_\alpha$ component obtained for the 1:10 turn MnZn ferrite sensor. The spectrum of the beta component $\mathbf{p}_\beta$ is identical to that of the alpha component shown above.

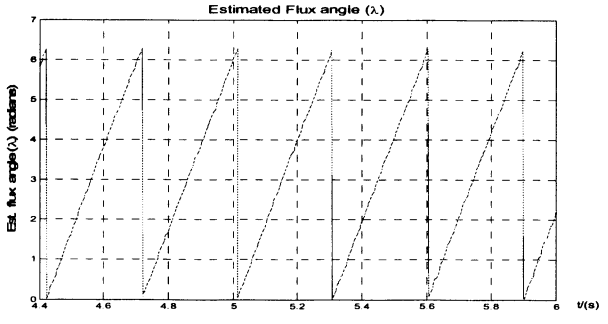

Fig.15. Resulting Flux position angle reconstructed from the 2λ angle obtained naturally from $\mathbf{p}_\alpha$ and $\mathbf{p}_\beta$ for the MnZn ferrite sensor.

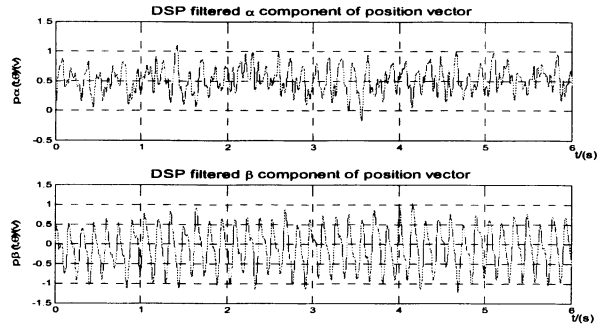

Fig.16. Quadrature components of the resulting position signal shown in the time domain obtained for the 1:100Turn off-the-shelf transducer.

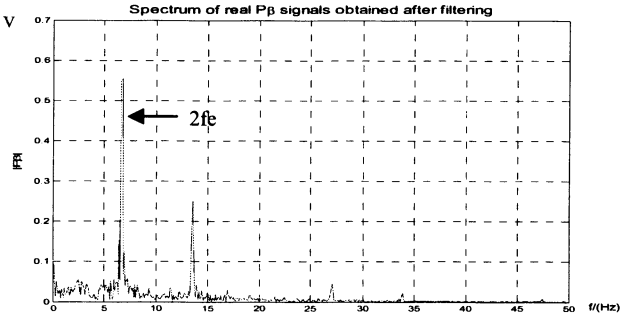

Fig.17. Spectrum of $\mathbf{p}_\beta$ component obtained for the 1:100Turn off the shelf transducer.

It is important to note that the settling time of the Coax CDS unlike the ferrite case, is very much a function of its damping resistance and termination impendence and therefore it must be matched accordingly.

7 Conclusions

This paper has investigated different types of current derivatives sensors that can be used for flux position estimation in standard induction motors using test vector application. Three main types of current derivative sensors were tested and implemented in practice. Results have shown flux position estimation suitable as the feedback signal for the control of the machine. The experimental results also showed that air-cored coaxial based-sensors require precise tuning [4] and matching before their implementation is effective (in the work presented this was achieved through experimentation). However their response is stable, and they do not suffer from saturation allowing them to be used on machines of different power rating. The other two sensors were based on high frequency ferrite cores. The output of these sensors yielded a larger output magnitude. However this signal might deteriorate due to saturation [6] under higher current transients. Thus the core material must be selected carefully depending on the power range of the motor involved.

References

[1] Caruana C. et al. "Sensorless flux position estimation at low and zero frequency by measuring Zero-Sequence Current in Delta Connected Cage Induction Machines" *IEEE Transactions on Industry Applications* Vol.41, Issue 2, March-April 2005 Page(s):609 – 617.

[2] Holtz J. and Juliet.J "Sensorless Acquisition of the rotor Position Angle for Induction Motors with arbitrary stator windings" *0-7803-8487-3/04 IEEE2004.*

[3] Holtz J., "Sensorless position control of induction motors-an emerging technology" *IEEE Transactions on Industrial Electronics* no6 vol45 pp840-852 Dec 1998.

[4] Ray,W.F and Davis R.M. " Wide Bandwidth Rogowski current transducers" part I- The Rogowski coil, EPE Journal 1/93 pp51-59.

[5] Schrödl M., "Sensorless Control of AC Machines at Low Speed and Standstill Based on the INFORM Method," *IEEE IAS Annual Meeting, San Diego, USA, Oct. 1996*, Vol. 1 pp. 270–277.

[6] Wolbank et al "Closed-Loop Compensating Sensors Versus new Current Derivative Sensors"*IEEE Transactions on Instrumentation and Measurement* Vol53 No.4 Aug 2004.